

# Geophysical Research Letters®

## RESEARCH LETTER

10.1029/2021GL095127

### Key Points:

- There are regional nonlinear changes as a function of global warming in CMIP5/6 precipitation, evaporation, and soil moisture projections
- Soil moisture shows the largest land fraction with nonlinear changes, but also the largest inter-model uncertainty
- Aerosols are responsible for some regional nonlinearities and might drive hydroclimate changes even as global temperature stabilizes

### Supporting Information:

Supporting Information may be found in the online version of this article.

### Correspondence to:

F. Lehner,  
[flavio.lehner@cornell.edu](mailto:flavio.lehner@cornell.edu)

### Citation:

Lehner, F., & Coats, S. (2021). Does regional hydroclimate change scale linearly with global warming? *Geophysical Research Letters*, 48, e2021GL095127. <https://doi.org/10.1029/2021GL095127>

Received 9 JUL 2021

Accepted 13 NOV 2021

### Author Contributions:

**Conceptualization:** Flavio Lehner, Sloan Coats

**Data curation:** Flavio Lehner, Sloan Coats

**Formal analysis:** Flavio Lehner

**Investigation:** Flavio Lehner, Sloan Coats

**Methodology:** Flavio Lehner, Sloan Coats

**Project Administration:** Flavio Lehner

**Visualization:** Flavio Lehner

**Writing – original draft:** Flavio Lehner

**Writing – review & editing:** Sloan Coats

## Does Regional Hydroclimate Change Scale Linearly With Global Warming?

Flavio Lehner<sup>1,2</sup>  and Sloan Coats<sup>3</sup>

<sup>1</sup>Department of Earth and Atmospheric Sciences, Cornell University, Ithaca, NY, USA, <sup>2</sup>Climate and Global Dynamics Laboratory, National Center for Atmospheric Research, Boulder, CO, USA, <sup>3</sup>Department of Earth Sciences, University of Hawaii, Honolulu, HI, USA

**Abstract** Many aspects of climate change scale linearly with global warming. However, nonlinear changes are possible, especially in the context of hydroclimate, and under emissions scenarios with stabilized global temperature, as aspired to by current climate targets. In CMIP5 and 6, a progressively larger land area shows nonlinear changes as a function of global warming when considering precipitation, evaporation, and soil moisture, with the latter showing nonlinearity over ~50% of global land. Using ensemble simulations with the Community Earth System Model 1, in which individual forcing factors are held constant, we illustrate how nonadditive responses to anthropogenic greenhouse gases and industrial and fire-related aerosols can yield complex soil moisture changes in certain regions. This complexity contributes to uncertainty in regional soil moisture projections and suggests that the timing of, as well as model response uncertainty to, future aerosol reductions will have significant impacts on regional hydroclimate change as global temperatures stabilize.

**Plain Language Summary** Current climate policy is focused on limiting global warming to certain levels, such as 1.5°C or 2°C. Most climate change assessments assume a linear relationship between the level of global warming and its impacts. However, we show that climate models project nonlinear changes of the regional hydrological cycle with warming and that aerosol emissions are a key driver of these nonlinearities. This means that, even if global temperature were to be stabilized by curbing greenhouse gas emissions, continuing changes in precipitation, evaporation, and soil moisture are possible as aerosol emissions continue to change.

## 1. Introduction

The aspirational climate target of limiting global warming to 1.5°C above preindustrial put a spotlight on low warming scenarios that were previously under-explored in climate change research (IPCC, 2018). It motivated the development of new climate model simulations designed to stabilize global warming at 1.5°C and 2°C (Mitchell et al., 2016; Sanderson et al., 2017), and also posed the challenge of assessing if climate change impacts differ significantly under a seemingly small 0.5°C difference in global warming (Schleussner et al., 2017; Seneviratne et al., 2018). Since only a small fraction of the Coupled Model Intercomparison Project (CMIP) Phase 5 and 6 simulations stabilize at 1.5°C or 2°C global warming, various sampling approaches have been applied to the CMIP archives in order to enable climate change impact assessments for these global warming targets (James et al., 2017). The most common approach is to extract a time window centered on 1.5°C or 2°C global warming, regardless of the underlying emissions scenario (Schleussner et al., 2016), as this is generally preferable to the classic pattern scaling approach (Herger et al., 2015). Consequently, for instance, a time window with 1.5°C global warming represents an earlier part of the 21st century under a high emissions scenario than a low emissions scenario (King, 2019; King et al., 2017). An important assumption of this approach is that climate change impacts scale with the level of global warming, irrespective of whether that level is transient or stable. This assumption has been shown to hold for many variables on global and regional scales (Seneviratne et al., 2016; Wartenburger et al., 2017), even as there are good reasons to assume that some do not (Good et al., 2016; King et al., 2019; Sniderman et al., 2019).

While the high and low emissions scenarios from CMIP5 and 6, Representative Concentration Pathway (RCP) 8.5 and Shared Socioeconomic Pathway (SSP) 5-8.5 and RCP 2.6 and SSP 1-2.6, respectively, portray very different emissions trajectories for greenhouse gases (GHGs), they all feature a decline in aerosol forcing due to the implementation of air pollution abatement measures with socioeconomic development (Lamarque et al., 2011;

Rao et al., 2017). “Time window” approaches, like those described above, implicitly ignore the role for aerosols in causing differing climate change impacts for the same global warming (Park et al., 2018). These approaches are expected to be particularly inaccurate where the response of the hydrological cycle depends on aerosol forcing (Lin et al., 2016; Pendergrass et al., 2015).

This issue is illustrated by 21st century changes in global land precipitation, evaporation, and total column soil moisture (hereafter soil moisture) in simulations with the Community Earth System Model version 1 (CESM1) (Figures 1a–1c). In CESM1 under RCP8.5, there is steady global warming to almost 5°C above the 1920–1949 mean by the end of the 21st century, while global land precipitation initially decreases due to the inhibiting effect of aerosols, before increasing at  $\sim 2.2\% \text{ C}^{-1}$  as the aerosol forcing declines (Figure 1a). Under scenarios that stabilize global warming at 1.5°C and 2°C through GHG mitigation, but retain the decline in aerosol forcing, global land precipitation increases even after global temperature has stabilized. For instance, if global land precipitation changes at 1.5°C or 2°C global warming are assessed using a “time window” approach under RCP8.5, in CESM1 they yield an increase of only 0.9% and 2.2% above the 1920–1949 mean. The same assessment under scenarios stabilized at 1.5°C and 2°C global warming, however, would yield an increase of 2.5% and 3.6%—because of the greater corresponding reduction in aerosol forcing (Figure 1a). This behavior is apparent in global land precipitation from other CMIP5 and 6 models, for instance, under the RCP8.5 and SSP5-8.5 scenarios as compared to lower emission scenarios like RCP2.6 and SSP1-2.6 (Figure 1a), as well as for other variables like global land evaporation, albeit with larger inter-model uncertainty (Figure 1b). Finally, global soil moisture also exhibits this behavior, with a tendency toward additional drying with stabilized global temperature (Figure 1c)—although, the inter-model uncertainty in soil moisture projections is particularly large. Regardless, these results suggest that individual forcing factors can drive a complex range of hydroclimate changes for the same global warming.

The above behavior has consequences for global warming target-based climate change impact assessments, and thus care must be taken when choosing data and methods for such assessments (James et al., 2017). In the context of hydroclimate, it also suggests that the common assumption of monotonic changes will not hold everywhere (Seager, 2015), and that the large-scale evolution of hydroclimate has been, and will continue to be, influenced by aerosol forcing (Bonfils et al., 2020; Marvel et al., 2019). By extension, this also means that observed hydroclimate changes (i.e., those associated with global warming from preindustrial to  $\sim 1^\circ\text{C}$ ), might not always be informative for constraining the characteristics of future changes. Indeed, in some regions, drought risk is not projected to change significantly from present day up to 2°C global warming, while large changes are projected under higher emissions (Lehner et al., 2017). Other work has highlighted how extreme precipitation depends nonlinearly on global warming (Pendergrass et al., 2019). Finally, projected aerosol-related changes in precipitation and potential evapotranspiration have been shown to balance each other at the global scale, yielding little net effect on aridity (aridity being precipitation divided by potential evapotranspiration), but that regionally, aridity can be strongly affected by aerosol forcing (Lin et al., 2016).

These results serve as a working hypothesis to investigate the potential for nonlinear hydroclimate changes as a function of global warming (hereafter referred to as nonlinear changes or nonlinearities). The aim of this paper is thus to identify nonlinearities (Sections 3.1 and 3.2), investigate the role of individual forcing factors and their potential non-additivity in driving those nonlinearities (Section 3.3), and discuss the implications of differences in forcing efficacy for warming targets (Section 4). It expands on earlier work by employing the full CMIP5 and CMIP6 ensembles, together with idealized simulations with CESM1 that isolate the influence of individual forcing factors.

## 2. Data and Methods

### 2.1. Model Simulations

We use several ensembles of simulations with CESM1 (Hurrell et al., 2013), all with the same component set in terms of resolution and physics: the CESM1 Large Ensemble, hereafter CESM1 ALL, consisting of 40 simulations run from 1920 to 2100 under “historical” and RCP8.5 forcing (Kay et al., 2015); and the CESM1 Low Warming simulations, consisting of 10 simulations each, stabilizing at 1.5°C and 2°C global warming above preindustrial conditions during the second half of the 21st century (Sanderson et al., 2017). To analyze individual forcing factors, we use two 20-member ensembles run from 1920 to 2080 with identical experimental setup and forcing as the CESM1 ALL, except that in one ensemble anthropogenic industrial aerosols are held constant at

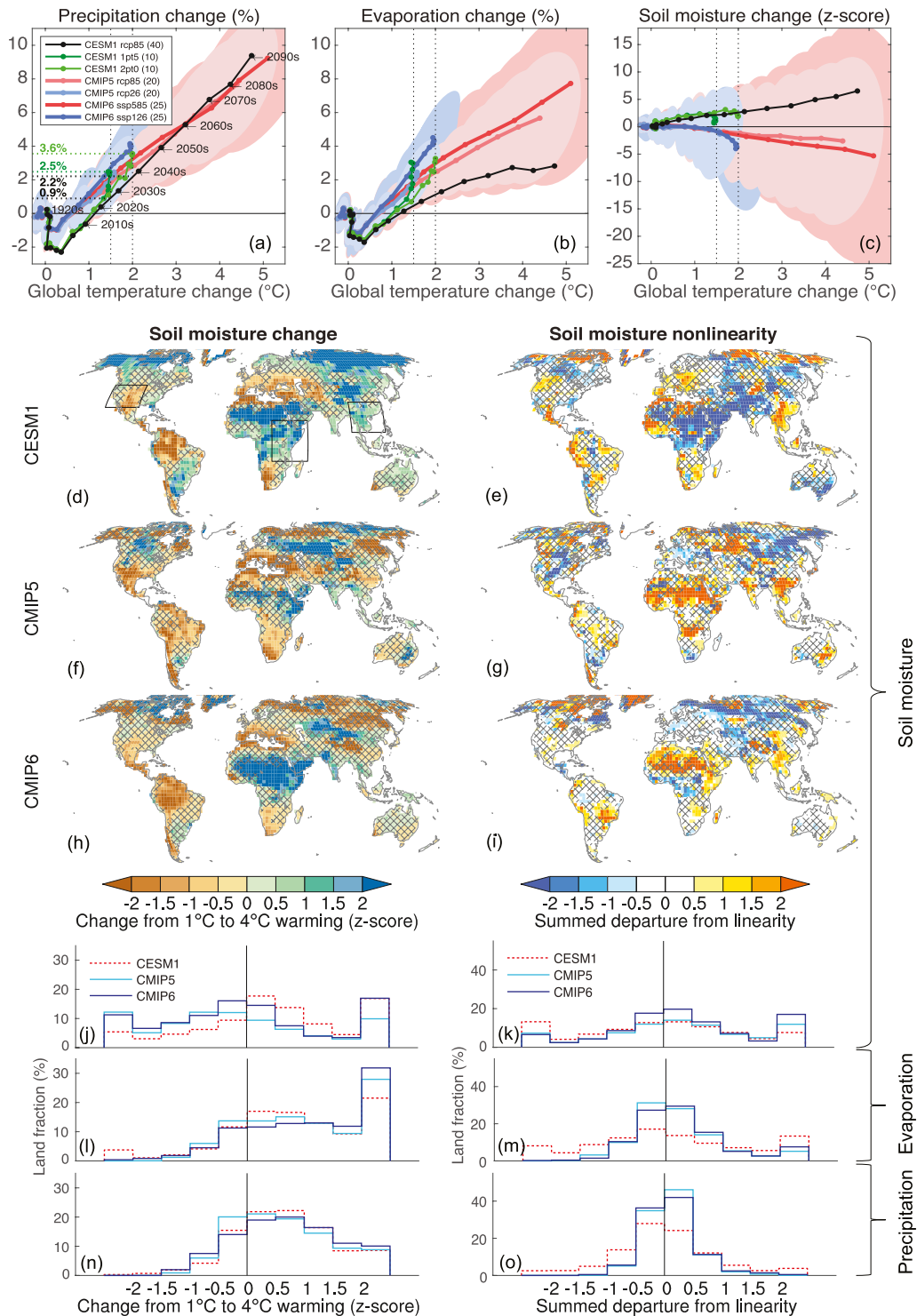


Figure 1.

1920 values (CESM1 XAER), while in the other ensemble greenhouse gases (GHGs) are held constant at 1920 values (CESM1 XGHG). An additional 15-member ensemble from 1920-2029 is used, in which aerosols from biomass burning are held constant at 1920 values (XBMB). The latter three ensembles are described in more detail in Deser et al. (2020). Note that in the CMIP protocol, aerosol forcing refers to the combination of anthropogenic industrial aerosols (AER) and biomass burning aerosols (BMB). The distinction between AER and BMB

in these ensembles enables understanding their relative contributions to the more commonly investigated total aerosol forcing.

To estimate the impact of individual forcing factors, we calculate  $AER = ALL - XAER$ ,  $GHG = ALL - XGHG$ , and  $BMB = ALL - XBMB$  using respective ensemble means. These residuals include possible nonlinear interactions between forcing factors, prompting us to investigate the additivity of the residuals explicitly (i.e., is  $ALL = AER + GHG + BMB$ ?). The ensembles do not cover forcing factors thought to be of lesser importance for secular hydroclimate trends, such as volcanic, solar, and ozone forcing, and land use change. The single-model individual forcing setup also enables a better sampling of internal variability, and thus more robust identification of the forced signal than would be possible using the CMIP multi-model ensembles (especially at regional scales), where only a few models provide single forcing simulations, often with only one ensemble member. On the other hand, this setup does not allow for an assessment of projection uncertainty due to model structural differences. We therefore contextualize the results from CESM1 with results from CMIP5 and 6.

## 2.2. Hydroclimate Metrics

To be consistent with previous studies of future hydroclimate (e.g., Cook et al., 2020), we use total column soil moisture (“mrso”), precipitation (“pr”), and evaporation (“hfls”) to characterize hydroclimate variability and change. Most time series are expressed as absolute anomalies (temperature) or relative anomalies (precipitation, evaporation) to the common reference period 1920–1949, except precipitation and evaporation are normalized (subtract mean and divide by standard deviation, SD) for the calculations in Section 2.4. Soil moisture, which has large inter-model spread in absolute values because of differing total soil column depths, is normalized over the reference period. Results are presented as annual means (January–December average).

## 2.3. Observational Data Sets and Model Evaluation

Due to the lack of spatially and temporally continuous observations of evaporation and soil moisture, it is difficult to comprehensively evaluate the simulation of regional hydroclimate by models (e.g., Ukkola et al., 2018). Nevertheless, to assess the realism of model-simulated hydroclimate, we use precipitation, evaporation, and total column soil moisture from 1950 to 2020 from the ERA5 data set (Hersbach et al., 2020).

## 2.4. Assessing the Linearity of Hydroclimate Changes as a Function of Global Warming

To assess whether hydroclimate changes are nonlinear as a function of global warming, we calculate the departure from linearity for a given increase in global temperature following King (2019):

$$D_{\Delta T} = \Delta Q_{\text{simulated to } \Delta T} - \frac{\Delta T}{\Delta T - \alpha} \Delta Q_{\text{simulated to } \Delta T - \alpha}$$

where  $\Delta Q$  is the change in a *normalized* hydroclimate metric (subtract mean and divide by SD) from 1920 to 1949 at each grid point,  $\Delta T$  is the change in global temperature from its 1920–1949 mean in °C, and  $\alpha$  is the  $\Delta T$  increment (here 1°C) over which the linearity is assessed. Departures from linearity are calculated for global warming of 2°C, 3°C and 4°C above 1920–1949 using 20-year mean time windows centered on the year closest to the respective warming level under the RCP8.5 and SSP5-8.5 scenarios.  $\Delta Q_{\text{simulated to } \Delta T}$  is calculated for the

**Figure 1.** (a) Global land precipitation changes as a function of global warming, relative to their 1920–1949 means, from CESM1 simulations under (black) RCP8.5 and (green and light green) 1.5°C and 2°C stabilization scenarios, as well as from (faint red and blue; one simulation per model) CMIP5 models under RCP8.5 and RCP2.6 and (red and blue) CMIP6 models under SSP5-8.5 and SSP1-2.6. Data plotted as nonoverlapping decadal means of annual means. For CMIP5 and CMIP6, an uncertainty range is given as a binomial probability distribution encompassing, on average, 50% of values for a given decadal mean. Number of ensemble members (CESM1) or models (CMIP5 and 6) is given in parentheses in panel (a). (b)–(c) Same as (a) but for global land evaporation and global total column soil moisture. Soil moisture is normalized relative to 1920–1949. (d) Change in normalized annual mean soil moisture for the 20-year period with ~4°C global warming relative to 1920–1949 in CESM1; hatching indicates differences that are not significant according to a two-sided *t* test (95% confidence level). (e) Summed departure from linearity as a function of global warming of 1°C, 2°C, 3°C, and 4°C; hatching indicates where the signal-to-noise ratio is smaller than one. Blue colors tend to indicate a convex trajectory with global warming, red colors a concave trajectory. (f)–(i) Same as (d)–(e) but for CMIP5 and 6; hatching indicates <67% models agree on the sign. (j–o) Histograms give the land fraction occupied by a certain color bar category for soil moisture, evaporation and precipitation (additional maps in Supporting Information S1).

same time windows for each ensemble member and CMIP model individually;  $\Delta Q_{\text{simulated to } \Delta T - \alpha}$  with  $\alpha = 1^\circ\text{C}$  is calculated analogously. Summing across the absolute value of the departure values for each global warming level ( $\sum |D_{\Delta T}|$ ) yields a summary measure for the nonlinearity of hydroclimate change for global warming from  $1^\circ\text{C}$  to  $4^\circ\text{C}$  (Figure S1 in Supporting Information S1). Summing across the actual departure values ( $\sum D_{\Delta T}$ ) indicates the magnitude and the shape of nonlinearity (Figures 1e, 1g and 1i). The metric  $\sum D_{\Delta T}$  takes into account the influence of internal variability by being considered robust when its ensemble mean value is larger than 1SD of its spread across ensemble members (in case of CESM1) or when more than 67% of models agree on the sign (in case of CMIP5 and 6). In observations from Berkeley Earth (Rohde et al., 2013) and HadCRUT5 (Morice et al., 2021) the period 1920–1949 is  $\sim 0.2^\circ\text{C}$  warmer than preindustrial (the 1850s); thus, the  $1^\circ\text{C}$  baseline used here corresponds closely to the observed warming to date since preindustrial of  $\sim 1.2^\circ\text{C}$ .

### 3. Results

#### 3.1. Linearity of Hydroclimate Changes

Consistent with previous studies using CESM1 and CMIP5 and 6, there is substantial soil moisture drying projected during the 21st century across many regions of the globe, in particular the Southwestern US, Central America, the Amazon, Southern Europe, South Africa, and Southern Australia (Figures 1d, 1f and 1h). Wetting is projected for East Africa, Central Asia, India, and Southern South America. CESM1 (Figure 1d) shows a similar pattern of soil moisture change as CMIP5 and 6 (Figures 1f and 1h), although it overall shows more wetting than either multimodel mean (Figure 1j), particularly at high latitudes, in East Asia, and Central Africa. Many of the regions with robust soil moisture drying also see robust precipitation declines, suggesting those as the main driver of soil moisture changes (Figure S1 in Supporting Information S1). Changes in total runoff, another major component of the terrestrial water budget, are tightly coupled to precipitation changes in many regions of the globe (not shown). However, the severity of, and land fraction with, soil moisture declines are overall larger than for precipitation, suggesting that increases in evaporation (Figure S3 in Supporting Information S1) act to amplify soil moisture drying (e.g., Cook et al., 2020).

Nonlinearities in the soil moisture changes show a complex pattern, with both convex and concave trajectories as a function of global warming (Figures 1d–1i). There is generally good correspondence between the summed departures and summed absolute values of departures from linearity as a function of global warming (Figure S1 in Supporting Information S1), such that we only show the summed departures in the main text. Across CESM1, CMIP5, and CMIP6, about 50% of the global land area (excluding Antarctica) shows nonlinearity of magnitude greater than 0.5 (Figure 1k). In CESM1, the largest coherent region of nonlinearity is a band from Central Africa to Southern Asia, South-East Asia, and the Maritime Continent (Figure 1e). CESM1, CMIP5, and CMIP6 show only limited consistency regarding the pattern of nonlinearity, although the general tendency for nonlinearity in the tropics exists in all three ensembles (Figures 1g and 1i). By contrast, evaporation shows a smaller land fraction with nonlinearities greater than 0.5 (Figure 1m) and an overall more consistent spatial pattern across the three ensembles (Figure S2 in Supporting Information S1). Precipitation shows the smallest land fraction with nonlinearities (Figure 1o and Figure S3 in Supporting Information S1). In other words, the land fraction with nonlinearities gradually increases when moving from precipitation to evaporation and then soil moisture, possibly because of the increasing complexity of processes shaping the response of these variables to forcing—which also manifest as larger model uncertainties in the associated projections (Figures 1a–1c).

In the following, three representative regions are investigated in more detail: South-East Asia, where the three ensembles do not agree on the sign of future soil moisture changes, but agree on the presence of nonlinearity with a convex trajectory, and where previous studies found a path-dependence of the precipitation response to the same warming level (Good et al., 2016); East Africa, where the models agree on a future wetting, but not on the presence of nonlinearity; and the Western United States, where there is no robust nonlinearity, but an earlier study with CESM1 found similar drying at both  $1.5^\circ\text{C}$  and  $2^\circ\text{C}$ , pointing to possible nonlinear responses under stabilized global temperatures (Lehner et al., 2017).

#### 3.2. Examples of Regional Hydroclimate Changes

While we illustrate hydroclimate changes as a function of global warming, very similar figures are obtained when using local instead of global temperature changes (Figure S4 in Supporting Information S1).

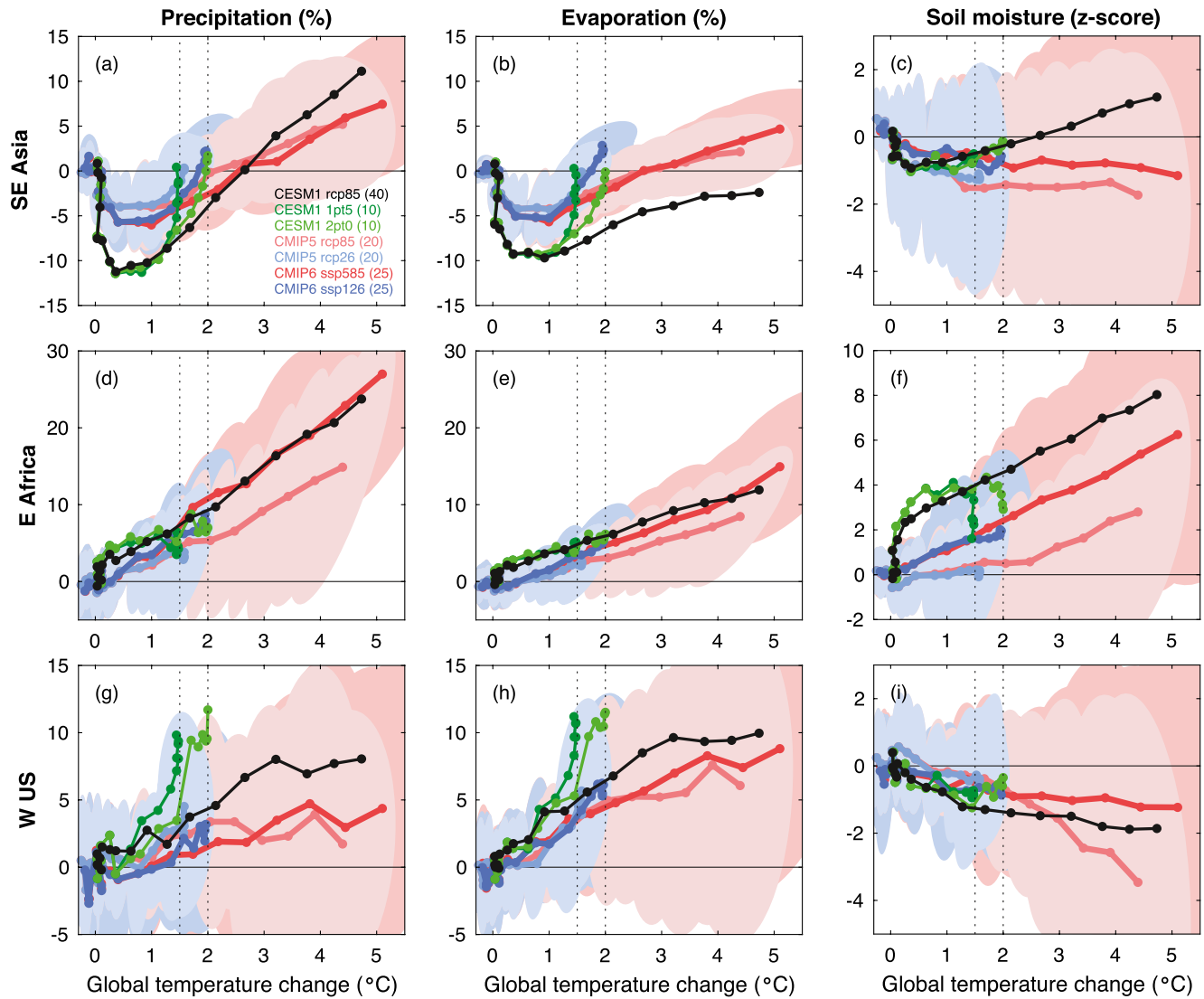


**Figure 2.** As Figures 1a–1c, but for (a–c) Southeast Asia, (d–f) East Africa, (g–i) Western United States.

In South-East Asia, strong nonlinearities in precipitation, evaporation, and soil moisture are simulated by all three ensembles (Figures 2a–2c). Each variable declines initially, despite global warming. In CMIP5 and 6, evaporation and precipitation recover quickly from the initial declines. However, the recovery of evaporation exceeds that of precipitation, leading to soil moisture declines, although these declines are relatively weak past 1.5°C global warming (Figure 2c). CESM1 ALL behaves similarly to CMIP5 and 6 initially (although with a larger magnitude), but evaporation never fully recovers, leading to soil moisture increases relative to the reference period (Figure 2c). Precipitation and evaporation in the 1.5°C and 2°C simulations with CESM1 show a clear deviation from CESM1 ALL, with a recovery back to reference period values after global temperature has stabilized (Figures 2a and 2b). However, these precipitation and evaporation changes largely balance each other, such that soil moisture remains comparable to CESM1 ALL at the same warming levels (Figure 2c).

In East Africa, all three ensembles project an increase of precipitation, evaporation, and soil moisture with global warming (Figures 2d–2f). However, CESM1 shows a sharp initial soil moisture increase, before any notable global warming (Figure 2f). This behavior is not seen in the CMIP5 and 6 multimodel means (although a small number of individual models exhibit similar behavior; not shown), which exhibit linearity for all scenarios and variables.

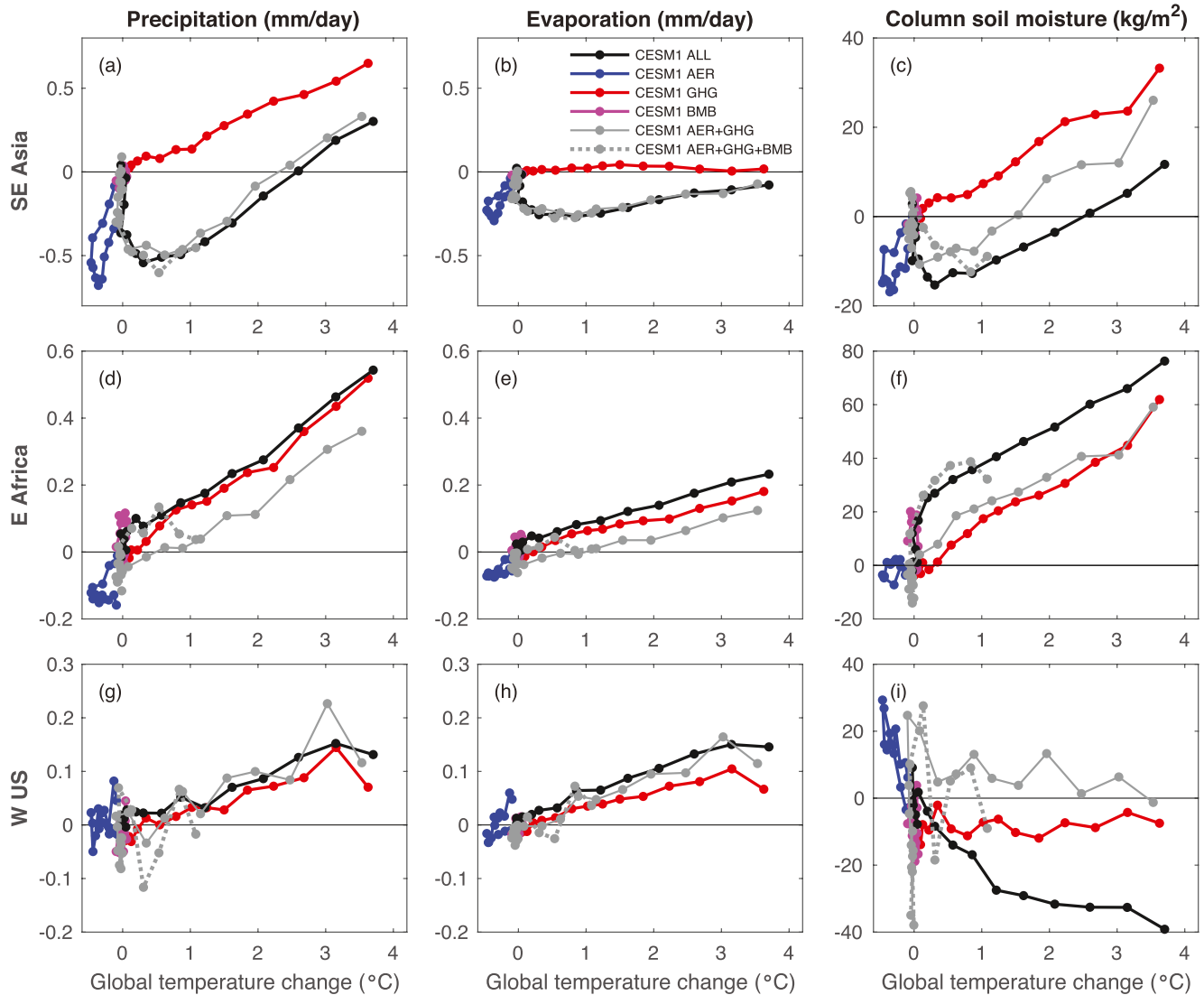


**Figure 3.** (a) Decadal ensemble mean of annual mean precipitation over South-East Asia, plotted as a function of the decadal ensemble mean of annual mean global temperature, from the CESM1 individual forcing factor ensembles, and combinations. Time series are relative to 1920–1949; the first decade is the 1920s, the last the 2080s, except for BMB and AER + GHG + BMB, which end with the 2020s. (b)–(c) Same as (a) but for evaporation and total column soil moisture. (d)–(f) and (g)–(i) same as (a)–(c) but for East Africa and Western United States.

In the Western United States, all three ensembles project increases in evaporation that outpace increases in precipitation, leading to soil moisture declines (Figures 2g–2i). There is a tendency for continued increases in precipitation and evaporation, even as global temperatures stabilize, although this response is significantly stronger in CESM1 than in CMIP5 and 6 (Figure 2g). Nevertheless, the precipitation and evaporation changes largely balance as global temperatures stabilize, leading to little additional soil moisture change (Figure 2i). For high emissions scenarios, however, there is a notable divergence of soil moisture changes among the three ensembles, with CMIP6 showing less drying than CMIP5, and with CESM1 sitting in between (Figure 2i).

### 3.3. The Role of Individual Forcing Factors and Their Additivity

To understand the role for individual forcing factors in driving the regional hydroclimate changes in the previous section, we examine the residual between the single forcing and ALL forcing simulations with CESM1 (e.g.,  $GHG = ALL - XGHG$ ) and plot them as a function of global warming (Figure 3). These residuals are shown as

absolute differences from to the reference period, to enable assessment of the additivity of the impacts of individual forcing factors, which is achieved by comparing GHG + AER + BMB to ALL.

In South-East Asia, the nonlinearity in precipitation, evaporation, and soil moisture in ALL occurs primarily due to AER (Figures 3a–3c). GHG drives a relatively linear increase in precipitation with global warming (Figure 3a; see Figure S5 in Supporting Information S1 for global maps), while having little impact on evaporation (Figure 3b and Figure S6 in Supporting Information S1), thus leading to a largely linear increase in soil moisture (Figure 3c and Figure S7 in Supporting Information S1). BMB does not play a significant role in South-East Asia. The impacts of the individual forcing factors are additive for precipitation and evaporation, but not as much for soil moisture. The general similarity of the CESM1 results with those from CMIP5 and 6 suggests that the importance of AER to South-East Asian hydroclimate change is robust across models. Indeed, idealized CMIP simulations with 1% CO<sub>2</sub> increase per year generally yield reduced nonlinearities over South-East Asia and other regions, confirming the role of aerosols in driving these nonlinearities (Figures S8–S10 in Supporting Information S1). Lending confidence to the real-world significance of these results, CESM1 tends to encompass observational estimates of precipitation, evaporation, and soil moisture over this region (Figure S11 in Supporting Information S1). However, there are also indications that the model is responding more strongly to aerosol forcing than is realistic (Figure S5 in Supporting Information S1).

In East Africa, nonlinearities in ALL are confined to the first ~1°C of global warming (Figures 3d–3f). Interestingly, these nonlinearities are, in part, related to BMB: precipitation increases about twice as much as evaporation due to BMB, leading to an increase in soil moisture before any notable global warming. Nevertheless, AER also contributes to nonlinearity by driving initial decreases in both precipitation and evaporation. These decreases, however, largely balance and thus occur without changes in soil moisture. It appears that the nonlinearities over East Africa in CESM1 ALL can be understood via two large-scale circulation responses to aerosols: the AER-induced relative cooling of the Northern Hemisphere drives a southward shift of the Inter Tropical Convergence Zone (e.g., Hwang et al., 2013), which decreases precipitation over East Africa (Figure S12 in Supporting Information S1). However, this drying is more than compensated for by increases in precipitation related to BMB, potentially via the Indian Ocean Dipole—BMB on Borneo warms the Eastern Indian Ocean, and cools the west, ultimately increasing precipitation over East Africa (Figure S12 in Supporting Information S1). The resulting increase in soil moisture in BMB, and in ALL, is at odds with observed soil moisture trends over East Africa (Figure S11 in Supporting Information S1). This model-data mismatch has been noted elsewhere (Tierney et al., 2015), and is an issue in other CMIP5 and 6 models, undermining confidence in the real world significance of these results.

In the Western United States, precipitation and evaporation increase linearly with global warming, with GHG being the main driver of these changes (Figures 3g and 3h). In ALL, evaporation increases slightly more than precipitation, leading to soil moisture declines. In GHG, however, the precipitation and evaporation increases largely balance, such that soil moisture does not change as significantly as in ALL. This is unexpected, as GHG-induced warming is widely viewed as being responsible for observed and projected soil moisture drying in the Western United States (e.g., Williams et al., 2020). Results from AER and BMB do not resolve this conundrum, as AER drives an increase in soil moisture and BMB has little influence. At the core of this conundrum is the fact that evaporation over the Western United States increases in all of the CESM1 single forcing ensembles, including those without notable warming (i.e., XGHG). The reasons for the evaporation increases, however, appear to be different for each forcing factor: in XAER, warming is the main driver of evaporation increases, while in XGHG, a positive anomaly in net cloud radiative forcing over the Western United States (mainly via a less negative short-wave forcing from reduced cloud cover) is likely responsible for increased evaporation (Figure S13 in Supporting Information S1). Consequently, all ensembles (XAER, XGHG, and XBMB) show a decline in soil moisture, such that the different forcing factors are not additive when considering soil moisture changes (Figure 3i). This, in turn, means that there are significant interactions between individual forcing factors in ALL that produce a soil moisture response resembling GHG-induced drying, but which cannot be isolated from these single forcing ensembles. Importantly, observational trends and variability in this region are generally well captured by CESM1 (Figure S11 in Supporting Information S1).

#### 4. Discussion and Conclusion

We provide evidence for nonlinear regional hydroclimate changes as a function of global warming in CMIP5 and 6 models as well as the CESM1 Large Ensemble. Using CESM1 single forcing simulations, we show that this behavior is often driven by regional aerosol forcing, consistent with existing literature on the importance of aerosol-driven regional climate change (Biasutti & Giannini, 2006; Feichter et al., 2004; Ming & Ramaswamy, 2009). A key result is that the land fraction affected by nonlinearity gradually increases from precipitation to evaporation to soil moisture. This suggests that the more complex and often nonlinear nature of processes underlying soil moisture, such as the vegetation response to CO<sub>2</sub> increases, produces a greater potential for nonlinear change, as well as nonadditivity of the impacts of individual forcing factors (see also Lemordant et al., 2018). A possible consequence of this is the larger model structural uncertainty for projections of land surface variables such as soil moisture (or runoff, e.g., Lehner et al., 2019), as compared to precipitation and evaporation, and future studies with seasonally resolved analysis are needed to draw inference about the exact processes leading to model discrepancy.

Separating industrial aerosols (AER) and biomass burning aerosols (BMB) reveals that these individual forcing factors can have distinct influences on regional hydroclimate. While AER can broadly be summarized as driving meridional forcing gradients, by cooling the Northern Hemisphere relative to the Southern Hemisphere, the historical and projected future hotspots of BMB are located primarily in the tropics, leading to zonal forcing gradients. This has an impact in East Africa, where meridional shifts in the ITCZ (primarily due to AER) and zonal shifts in IOD-related sea surface temperatures (primarily due to BMB) lead to nonlinear hydroclimate changes in CESM1. Confidence in the real-world significance of these results will require that AER and BMB also drive distinct regional hydroclimate changes in other models. However, confirming this is not currently possible, as the separation of AER and BMB is not part of the Detection and Attribution Model Intercomparison Project protocol (Gillett et al., 2016). Further undermining confidence, observed hydroclimate trends in East Africa appear at odds with those simulated by models.

It is important to note that while the sensitivity to global aerosol forcing in CESM1 falls in the middle of the CMIP5 model cohort (Bellouin et al., 2020; Zelinka et al., 2014), CESM1's regional aerosol forcing, in particular of precipitation and evaporation, appears to be stronger than the average CMIP5 and 6 model, and at times stronger than observational estimates. Nevertheless, it remains challenging to validate the regional aerosol forcing of hydroclimate in climate models due to the small signal-to-noise ratio in observations over the 20th century. This is consistent with recent detection and attribution studies that were able to parse the influence of aerosols on observed hydroclimate globally, but not regionally (Bonfils et al., 2020; Marvel et al., 2019, 2020).

The confounding influence of aerosols on GHG-driven climate trends has long been discussed, although mostly in the context of the historical record (Dong & Sutton, 2015; Lau & Kim, 2017). Less attention has been paid to the role of aerosols in driving future climate changes, in particular, in scenarios with stabilized global temperatures (Sanderson et al., 2017; Scannell et al., 2019). Here, we demonstrate that the expected future reduction in aerosol forcing can drive regional hydroclimate changes, such that these changes do not scale linearly with global warming, and that the previously known efficacy difference of aerosol and GHG forcing extend beyond precipitation (Feichter et al., 2004). CESM1 provides a relatively extreme case study with sometimes substantial changes of precipitation, evaporation, and soil moisture *after* global temperatures have been stabilized. Similar behavior is seen in low emissions scenarios in CMIP5 and 6, although with large inter-model differences. We speculate that these differences are, to first order, due to uncertainties in the sensitivity of models to global and regional aerosol forcing, although differing timescales of ocean heat uptake and sea surface temperature equilibration after GHG mitigation likely also play a role (MacDougall et al., 2020; Sniderman et al., 2019). Assuming successful GHG mitigation, the regional hydroclimate response to reductions in aerosols may need to come into greater focus.

#### Data Availability Statement

All CESM1 simulations are available at <https://www.earthsystemgrid.org>. CMIP simulations are available through PCMDI at <https://esgf-node.llnl.gov>. All observations are available from the respective institution's website (ERA5: <https://www.ecmwf.int/en/forecasts/datasets/reanalysis-datasets/era5>; Berkeley Earth: <http://berkeley-earth.org/data/>; HadCRUT5: <https://www.metoffice.gov.uk/hadobs/hadcrut5/data/current/download.html>).

### Acknowledgments

The authors thank Angeline Pendergrass, Isla Simpson, Pedro DiNezio and Clara Deser for discussion and two anonymous reviewers for constructive feedback. The authors acknowledge the efforts of all those who contributed to producing the simulations and observational data sets, in particular Dani Coleman, Nan Rosenbloom and Isla Simpson for producing the single forcing simulations with CESM1. Flavio Lehner was supported by NSF AGS-0856145 Amendment 87, by the Bureau of Reclamation under Cooperative Agreement R16AC00039, the Regional and Global Model Analysis (RGMA) component of the Earth and Environmental System Modeling Program of the U.S. Department of Energy's Office of Biological & Environmental Research (BER) Cooperative Agreement DE-FC02-97ER62402, and a Swiss NSF Ambizione Fellowship (Project PZ00P2\_174128). This is SOEST publication no. 11442.

### References

- Bellouin, N., Quaas, J., Gryspeerdt, E., Kinne, S., Stier, P., Watson-Parris, D., et al. (2020). Bounding global aerosol radiative forcing of climate change. *Reviews of Geophysics*, *58*, 1–45. <https://doi.org/10.1029/2019RG000660>
- Biasutti, M., & Giannini, A. (2006). Robust Sahel drying in response to late 20th century forcings. *Geophysical Research Letters*, *33*, 10–13. <https://doi.org/10.1029/2006GL026067>
- Bonfils, C. J. W., Santer, B. D., Fyfe, J. C., Marvel, K., Phillips, T. J., & Zimmerman, S. R. H. (2020). Human influence on joint changes in temperature, rainfall and continental aridity. *Nature Climate Change*, *10*, 726–731. <https://doi.org/10.1038/s41558-020-0821-1>
- Cook, B. I., Mankin, J. S., Marvel, K., Williams, A. P., Smerdon, J. E., & Anchukaitis, K. J. (2020). Twenty-first century drought projections in the CMIP6 forcing scenarios. *Earth's Future*, *8*, e2019EF001461. <https://doi.org/10.1029/2019EF001461>
- Deser, C., Phillips, A. S., Simpson, I. R., Rosenbloom, N., Coleman, D., Lehner, F., et al. (2020). Isolating the evolving contributions of anthropogenic aerosols and greenhouse gases in the CESM1 large ensemble with single-forcing simulations. *Journal of Climate*, *33*(18), 7835–7858. <https://doi.org/10.1175/JCLI-D-20-0123.1>
- Dong, B., & Sutton, R. (2015). Dominant role of greenhouse-gas forcing in the recovery of Sahel rainfall. *Nature Climate Change*, *5*, 757–760. <https://doi.org/10.1038/nclimate2664>
- Feichter, J., Roeckner, E., Lohmann, U., & Liepert, B. (2004). Nonlinear aspects of the climate response to Greenhouse gas and aerosol forcing. *Journal of Climate*, *17*, 2384–2398. [https://doi.org/10.1175/1520-0442\(2004\)017<2384:NAOTCR>2.0.CO;2](https://doi.org/10.1175/1520-0442(2004)017<2384:NAOTCR>2.0.CO;2)
- Gillett, N. P., Shiogama, H., Funke, B., Hegerl, G., Knutti, R., Matthes, K., et al. (2016). The Detection and Attribution Model Intercomparison Project (DAMIP v1.0) contribution to CMIP6. *Geoscientific Model Development*, *9*, 3685–3697. <https://doi.org/10.5194/gmd-9-3685-2016>
- Good, P., Booth, B. B. B., Chadwick, R., Hawkins, E., Jonko, A., & Lowe, J. A. (2016). Large differences in regional precipitation change between a first and second 2 K of global warming. *Nature Communications*, *7*, 1–8. <https://doi.org/10.1038/ncomms13667>
- Herger, N., Sanderson, B. M., & Knutti, R. (2015). Improved pattern scaling approaches for the use in climate impact studies. *Geophysical Research Letters*, *42*, 3486–3494. <https://doi.org/10.1002/2015GL063569>
- Hersbach, H., Bell, B., Berrisford, P., Hirahara, S., Horányi, A., Muñoz-Sabater, J., et al. (2020). The ERA5 global reanalysis. *Quarterly Journal of the Royal Meteorological Society*, *146*, 1999–2049. <https://doi.org/10.1002/qj.3803>
- Hurrell, J. W., Holland, M. M., Gent, P. R., Ghan, S., Kay, J. E., Kushner, P. J., et al. (2013). The community earth system model: A framework for collaborative research. *Bulletin of the American Meteorological Society*, *94*, 1339–1360. <https://doi.org/10.1175/BAMS-D-12-00121.1>
- Hwang, Y. T., Frierson, D. M. W., & Kang, S. M. (2013). Anthropogenic sulfate aerosol and the southward shift of tropical precipitation in the late 20th century. *Geophysical Research Letters*, *40*, 2845–2850. <https://doi.org/10.1002/grl.50502>
- IPCC. (2018). Summary for Policymakers. In *Global warming of 1.5°C. An IPCC Special Report on the impacts of global warming of 1.5°C above pre-industrial levels and related global greenhouse gas emission pathways, in the context of strengthening the global response to the threat of climate change*.
- James, R., Washington, R., Schleussner, C. F., Rogelj, J., & Conway, D. (2017). Characterizing half-a-degree difference: A review of methods for identifying regional climate responses to global warming targets. *Wiley Interdisciplinary Reviews: Climate Change*, *8*, e457. <https://doi.org/10.1002/wcc.457>
- Kay, J. E., Deser, C., Phillips, A., Mai, A., Hannay, C., Strand, G., et al. (2015). The community earth system model (CESM) large ensemble project: A community resource for studying climate change in the presence of internal climate variability. *Bulletin of the American Meteorological Society*, *96*, 1333–1349. <https://doi.org/10.1175/BAMS-D-13-00255.1>
- King, A. (2019). The drivers of nonlinear local temperature change under global warming. *Environmental Research Letters*, *14*, 064005. <https://doi.org/10.1088/1748-9326/ab1976>
- King, A. D., Karoly, D. J., & Henley, B. J. (2017). Australian climate extremes at 1.5°C and 2°C of global warming. *Nature Climate Change*, *7*, 412–416. <https://doi.org/10.1038/nclimate3296>
- King, A. D., Lane, T. P., Henley, B. J., & Brown, J. R. (2019). Global and regional impacts differ between transient and equilibrium warmer worlds. *Nature Climate Change*, *10*, 42–47. <https://doi.org/10.1038/s41558-019-0658-7>
- Lamarque, J. F., Kyle, P. P., Meinshausen, M., Riahi, K., Smith, S. J., van Vuuren, D. P., et al. (2011). Global and regional evolution of short-lived radiatively-active gases and aerosols in the representative concentration pathways. *Climate Change*, *109*, 191–212. <https://doi.org/10.1007/s10584-011-0155-0>
- Lau, W. K. M., & Kim, K. M. (2017). Competing influences of greenhouse warming and aerosols on Asian summer monsoon circulation and rainfall. *Asia-Pacific Journal of Atmospheric Sciences*, *53*, 181–194. <https://doi.org/10.1007/s13143-017-0033-4>
- Lehner, F., Coats, S., Stocker, T. F., Pendergrass, A. G., Sanderson, B. M., Raible, C. C., & Smerdon, J. E. (2017). Projected drought risk in 1.5°C and 2°C warmer climates. *Geophysical Research Letters*, *44*, 7419–7428. <https://doi.org/10.1002/2017GL074117>
- Lehner, F., Wood, A. W., Vano, J. A., Lawrence, D. M., Clark, M. P., & Mankin, J. S. (2019). The potential to reduce uncertainty in regional runoff projections from climate models. *Nature Climate Change*, *9*, 926–933. <https://doi.org/10.1038/s41558-019-0639-x>
- Lemordant, L., Gentine, P., Swann, A. S., Cook, B. I., & Scheff, J. (2018). Critical impact of vegetation physiology on the continental hydrologic cycle in response to increasing CO<sub>2</sub>. *Proceedings of the National Academy of Sciences of United States of America*, *115*, 4093–4098. <https://doi.org/10.1073/pnas.1720712115>
- Lin, L., Gettelman, A., Fu, Q., & Xu, Y. (2016). Simulated differences in 21st century aridity due to different scenarios of greenhouse gases and aerosols. *Climate Change*, *146*, 1–422. <https://doi.org/10.1007/s10584-016-1615-3>
- MacDougall, A. H., Frölicher, T. L., Jones, C. D., Rogelj, J., Matthews, H. D., Zickfeld, K., et al. (2020). Is there warming in the pipeline? A multi-model analysis of the Zero Emissions Commitment from CO<sub>2</sub>. *Biogeosciences*, *17*, 2987–3016. <https://doi.org/10.5194/bg-17-2987-2020>
- Marvel, K., Biasutti, M., & Bonfils, C. (2020). Fingerprints of external forcings on Sahel rainfall: Aerosols, greenhouse gases, and model-observation discrepancies. *Environmental Research Letters*, *15*, 084023. <https://doi.org/10.1088/1748-9326/ab858e>
- Marvel, K., Cook, B. I., Bonfils, C. J. W., Durack, P. J., Smerdon, J. E., & Williams, A. P. (2019). Twentieth-century hydroclimate changes consistent with human influence. *Nature*, *569*, 59–65. <https://doi.org/10.1038/s41586-019-1149-8>
- Ming, Y., & Ramaswamy, V. (2009). Nonlinear climate and hydrological responses to aerosol effects. *Journal of Climate*, *22*, 1329–1339. <https://doi.org/10.1175/2008JCLI2362.1>
- Mitchell, D., AchutaRao, K., Allen, M., Bethke, I., Forster, P., Fuglestedt, J., et al. (2017). Half a degree Additional warming, Projections, Diagnosis and Impacts (HADPI): Background and experimental design. *Geoscientific Model Development Discussions*, *10*(2), 571–583. <https://doi.org/10.5194/gmd-2016-203>
- Morice, C. P., Kennedy, J. J., Rayner, N. A., Winn, J. P., Hogan, E., Killick, R. E., et al. (2021). An updated assessment of near-surface temperature change from 1850: The HadCRUT5 dataset. *Journal of Geophysical Research: Atmospheres*, *126*(3), e2019JD032361. <https://doi.org/10.1029/2019JD032361>

- Park, C. E., Jeong, S.-J., Joshi, M., Osborn, T. J., Ho, C.-H., Piao, S., et al. (2018). Keeping global warming within 1.5°C constrains emergence of aridification. *Nature Climate Change*, 8, 70–74. <https://doi.org/10.1038/s41558-017-0034-4>
- Pendergrass, A. G., Coleman, D. B., Deser, C., Lehner, F., Rosenbloom, N., & Simpson, I. R. (2019). Nonlinear Response of Extreme Precipitation to Warming in CESM1. *Geophysical Research Letters*, 46, 10551–10560. <https://doi.org/10.1029/2019GL084826>
- Pendergrass, A. G., Lehner, F., Sanderson, B. M., & Xu, Y. (2015). Does extreme precipitation intensity depend on the emissions scenario? *Geophysical Research Letters*, 42, 8767–8774. <https://doi.org/10.1002/2015GL065854>
- Rao, S., Kilmont, Z., Smith, S. J., Van Dingenen, R., Dentener, F., Bouwman, L., et al. (2017). Future air pollution in the shared socio-economic pathways. *Global Environmental Change*, 42, 346–358. <https://doi.org/10.1016/j.gloenvcha.2016.05.012>
- Rohde, R., & Muller, R., Jacobsen, R., Perlmutter, S., Rosenfeld, A., Wurtele, J., et al. (2013). Berkeley Earth temperature averaging process. *Geoinformatics & Geostatistics: An Overview*, 1, 1–13. <https://doi.org/10.4172/2327-4581.1000103>
- Sanderson, B. M., Xu, Y., Tebaldi, C., Wehner, M., O'Neill, B., Jahn, A., et al. (2017). Community climate simulations to assess avoided impacts in 1.5 and 2°C futures. *Earth System Dynamics*, 8, 827–847. <https://doi.org/10.5194/esd-8-827-2017>
- Scannell, C., Booth, B. B. B., Dunstone, N. J., Rowell, D. P., Bernie, D. J., Kasoar, M., et al. (2019). The influence of remote aerosol forcing from industrialized economies on the future evolution of East and West African rainfall. *Journal of Climate*, 32, 8335–8354. <https://doi.org/10.1175/JCLI-D-18-0716.1>
- Schleussner, C. F., Lissner, T. K., Fischer, E. M., Wohland, J., Perrette, M., Golly, A., et al. (2016). Differential climate impacts for policy-relevant limits to global warming: The case of 1.5°C and 2°C. *Earth System Dynamics*, 7, 327–351. <https://doi.org/10.5194/esd-7-327-2016>
- Schleussner, C.-F., Pfleiderer, P., & Fischer, E. M. (2017). In the observational record half a degree matters. *Nature Climate Change*, 7, 460–462. <https://doi.org/10.1038/nclimate3320>
- Seager, R. (2015). Decadal hydroclimate variability across the Americas. In C.-P. Chang, M. Ghil, M. Latif, & J. M. Wallace (Eds.), *Climate change: Multidecadal and beyond* (p. 388). World Scientific.
- Seneviratne, S. I., Donat, M. G., Pitman, A. J., Knutti, R., & Wilby, R. L. (2016). Allowable CO<sub>2</sub> emissions based on regional and impact-related climate targets. *Nature*, 529, 477–483. <https://doi.org/10.1038/nature16542>
- Seneviratne, S. I., Rogelj, J., Séférian, R., Wartenburger, R., Allen, M. R., Cain, M., et al. (2018). The many possible climates from the Paris Agreement's aim of 1.5°C warming. *Nature*, 558, 41–49. <https://doi.org/10.1038/s41586-018-0181-4>
- Sniderman, J. M. K., Brown, J. R., Woodhead, J. D., King, A. D., Gillett, N. P., Tokarska, K. B., et al. (2019). Southern Hemisphere subtropical drying as a transient response to warming. *Nature Climate Change*, 9, 232–236. <https://doi.org/10.1038/s41558-019-0397-9>
- Tierney, J. E., Ummenhofer, C. C., & DeMenocal, P. B. (2015). Past and future rainfall in the Horn of Africa. *Science Advances*, 1, e1500682. <https://doi.org/10.1126/sciadv.1500682>
- Ukkola, A. M., Pitman, A. J., De Kauwe, M. G., Abramowitz, G., Herger, N., Evans, J. P., & Decker, M. (2018). Evaluating CMIP5 model agreement for multiple drought metrics. *Journal of Hydrometeorology*, 19, 969–988. <https://doi.org/10.1175/JHM-D-17-0099.1>
- Wartenburger, R., Hirschi, M., Donat, M. G., Greve, P., Pitman, A. J., & Seneviratne, S. I. (2017). Changes in regional climate extremes as a function of global mean temperature: An interactive plotting framework. *Geoscientific Model Development*, 10, 3609–3634. <https://doi.org/10.5194/gmd-10-3609-2017>
- Williams, A. P., Cook, E. R., Smerdon, J. E., Cook, B. I., Abatzoglou, J. T., Bolles, K., et al. (2020). Large contribution from anthropogenic warming to an emerging North American megadrought. *Science*, 368, 314–318. <https://doi.org/10.1126/science.aaz9600>
- Zelinka, M. D., Andrews, T., Forster, P. M., & Taylor, K. E. (2014). Quantifying components of aerosol-cloud-radiation interactions in climate models. *Journal of Geophysical Research: Atmospheres*, 119, 7599–7615. <https://doi.org/10.1002/2014JD021710>